RESEARCH ARTICLE

AMERICAN JOURNAL OF medical genetics PART A

Early Presentation of Cystic Kidneys in a Family With a Homozygous *INVS* Mutation

Machteld M. Oud,[1,2,3] Bregje W. van Bon,[1] Ernie M. H. F. Bongers,[1] Alexander Hoischen,[1,3] Carlo L. Marcelis,[1] Nicole de Leeuw,[1,2,3] Suzanne J. J. Mol,[4] Geert Mortier,[5] Nine V. A. M. Knoers,[6] Han G. Brunner,[1,2,3] Ronald Roepman,[1,2,3] and Heleen H. Arts[1,2,3]*

[1]Department of Human Genetics, Radboud University Medical Centre, Nijmegen, The Netherlands

[2]Radboud Institute for Health Sciences, Radboud University Medical Centre, Nijmegen, The Netherlands

[3]Radboud Institute for Molecular Life Sciences, Radboud University Nijmegen, Nijmegen, The Netherlands

[4]Department of Pathology, Jeroen Bosch Hospital, 's-Hertogenbosch, The Netherlands

[5]Department of Medical Genetics, Antwerp University Hospital and University of Antwerp, Edegem, Belgium

[6]Department of Medical Genetics, University Medical Centre Utrecht, Utrecht, The Netherlands

Manuscript Received: 26 March 2013; Manuscript Accepted: 27 January 2014

Nephronophthisis (NPHP) is an autosomal recessive cystic kidney disease that is the most frequent monogenic cause of end-stage renal disease in children. Infantile NPHP, often in combination with other features like *situs inversus*, are commonly caused by mutations in the *INVS* gene. *INVS* encodes the ciliary protein inversin, and mutations induce dysfunction of the primary cilia. In this article, we present a family with two severely affected fetuses that were aborted after discovery of grossly enlarged cystic kidneys by ultrasonography before 22 weeks gestation. Exome sequencing showed that the fetuses were homozygous for a previously unreported nonsense mutation, resulting in a truncation in the IQ1 domain of inversin. This mutation induces nonsense-mediated RNA decay, as suggested by a reduced RNA level in fibroblasts derived from the fetus. However, a significant amount of mutant *INVS* RNA was present in these fibroblasts, yielding mutant inversin protein that was mislocalized. In control fibroblasts, inversin was present in the ciliary axoneme as well as at the basal body, whereas in the fibroblasts from the fetus, inversin could only be detected at the basal body. The phenotype of both fetuses is partly characteristic of infantile NPHP and Potter sequence. We also identified that the fetuses had mild skeletal abnormalities, including shortening and bowing of long bones, which may expand the phenotypic spectrum associated with *INVS* mutations.

Key words: Infantile NPHP; Potter sequence; *INVS*

How to Cite this Article:
Oud MM, van Bon BW, Bongers EMHF, Hoischen A, Marcelis CL, de Leeuw N, Mol SJJ, Mortier G, Knoers NVAM, Brunner HG, Roepman R, Arts HH. 2014. Early presentation of cystic kidneys in a family with a homozygous *INVS* mutation.
Am J Med Genet Part A 164A:1627–1634.

INTRODUCTION

Nephronophthisis (NPHP) is an autosomal recessively inherited cystic kidney disease, and one of the most frequent monogenic disorders that causes end-stage renal disease (ESRD) in children and adolescents [Hildebrandt and Otto, 2005]. Three phenotypic variants of NPHP have been described, taking into account the age of onset for ESRD; the infantile, the juvenile, and the adolescent variant [Saunier et al., 2005]. To date, mutations in at least 14 genes are associated with any of the three variants, explaining 40% of the cases, rendering NPHP as a genetically heterogeneous disorder [Hurd and Hildebrandt, 2011; Arts and Knoers, 2012; Halbritter et al., 2013]. Infantile NPHP is the most progressive variant and has

Grant sponsor: Dutch Kidney Foundation; Grant numbers: KJPB09.009, IP11.58, CP11.18; Grant sponsor: The Netherlands Organization for Health Research and Development; Grant numbers: ZonMW Veni-91612095, ZonMW Veni-91613008; Grant sponsor: The Netherlands Organization for Scientific Research; Grant numbers: NWO Vidi-91786396, Vici-016130664.

*Correspondence to:
Heleen H. Arts, Department of Human Genetics-855, Radboud Institute for Molecular Life Sciences, Radboud University Medical Centre, PO-Box 9101, 6500HB Nijmegen, The Netherlands.
E-mail: heleen.arts@radboudumc.nl

Article first published online in Wiley Online Library (wileyonlinelibrary.com): 26 March 2014
DOI 10.1002/ajmg.a.36501

an early onset of ESRD before the age of 2 years. In infantile NPHP the kidneys are often significantly enlarged due to cortical cysts, and patients often show hepatic fibrosis. Two other features commonly found in patients with infantile NPHP are *situs inversus* and cardiac ventricular septal defects. Histological findings in infantile NPHP differ from juvenile and adolescent NPHP, in the fact that thickening of the tubular basement membrane is rarely found [Gagnadoux et al., 1989; Tory et al., 2009]. Thus far, only two genes, *INVS* and *NPHP3*, have been associated with infantile NPHP. Patients with mutations in *INVS* have a more severe kidney phenotype, and the progression toward ESRD in these patients is faster than in patients with a mutation in *NPHP3* [Otto et al., 2003; Tory et al., 2009]. The phenotypic spectrum associated with *INVS* mutations ranges from ESRD in combination with hepatic fibrosis and *situs inversus* to a syndrome with respiratory failure and oligohydramnios that resembles Potter sequence [Haider et al., 1998]. Potter sequence or Potter syndrome, first described by Edith L. Potter in 1946, is characterized by severe oligohydramnios causing pulmonary hypoplasia, and facial dysmorphism also known as a Potter facies [Thomas and Smith, 1974]. In this article, we present a family with two severely affected fetuses. Pathological examination showed enlarged cystic kidneys, liver fibrosis, oligohydramnios, and suspected skeletal abnormalities. Exome sequencing (ES) demonstrated that both fetuses had a previously unreported homozygous nonsense mutation in *INVS* that predicted a truncation of the IQ1 domain of inversin.

CLINICAL REPORT

In this family there were four pregnancies of which two were terminated before gestational week 22 (Fig. 1A). The pregnancies of individuals II:1 and II:4 were complicated by oligohydramnios, with small lungs and a flattened nose. Both individuals, II:1 and II:4, had grossly enlarged cystic kidneys that were detected by ultrasonography (Fig. 1D–F). Pathologic examination of individual II:1 showed *situs inversus* of the lungs, dextroversion, a cystic liver with fibrosis, and possible shortening and mild bowing of the femora (Fig. 1). An overview of all clinical features of both fetuses is given in Table I, while Table II shows the body parameters and organ weights of both fetuses. Histological features of the renal cortex of individual II:1 included multiple dilated cystic ductal structures and dilated glomerular cysts (Fig. 2A,B). Thickening of the tubular basement membrane was absent in the renal cortex of individual II:1 (Fig. 2C). Sections of the liver of individual II:1 showed congenital hepatic fibrosis, dilated cystic biliary structures, and ductal plate malformation (Fig. 2D). DNA and histological- or radiographic records were unavailable for individual II:4, although these were requested at the time of autopsy.

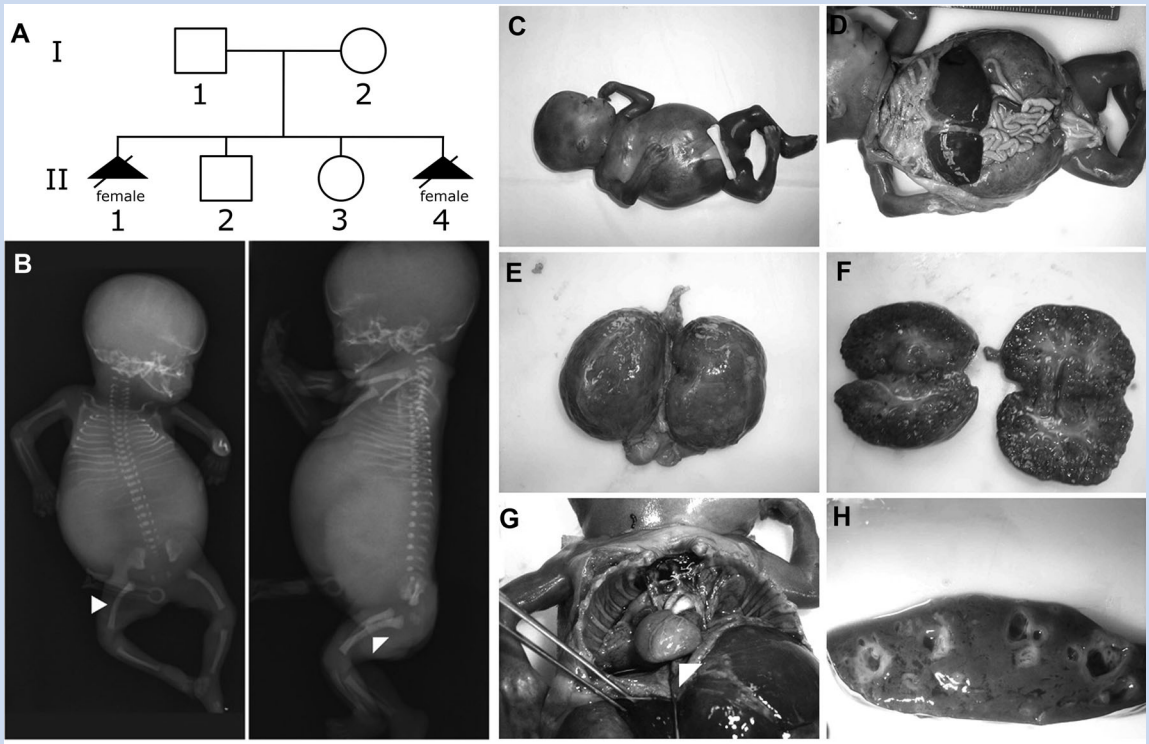

FIG. 1. A: Pedigree of present family. B: Radiographs of fetus II:1 showing a narrow thorax and possible shortening and mild bowing of the femora (indicated by arrowheads). C–H: Pathological images of fetus II:1. C, D: The enlargement of the belly is due to the grossly enlarged kidneys. All organs are present. E, F: Enlarged cystic kidneys. G: Dextroversion (indicated by arrowhead). H: Cystic and fibrotic liver. The family provided written informed consent for publication of clinical images.

TABLE I. Clinical Features of the Present Family and Three Individuals From the Bedouin Family Described by Haider et al. [1998]

	Present family		Haider et al. [1998]		
Features	**II:1**	**II:4**	**VII:1**	**VII:3**	**VII:18**
Gestational age (weeks)	22	16	Term	Term	Term
Gender	F	F	M	F	M
Age at onset NPHP (years)	NA	NA	2.5	2.5	0
Enlarged cystic kidneys	+++	+	+	+	++
End-stage renal disease	NA	NA	+	+	+
Oligohydramnios	++	+	−	−	+
Flattened nose	+	NS	NS	NS	NS
Narrow thorax	+	NS	NS	NS	NS
Respiratory failure	NA	NA	−	−	+
Pulmonary hypoplasia	++	+	NS	NS	NS
Anemia	NA	NA	+	+	NA
Situs inversus of the lungs	+	NS	NS	NS	NS
Dextroversion	+	NS	NS	NS	NS
Enlarged cystic liver	+	−	−	−	−
Congenital liver fibrosis	+	+	NS	NS	NS
Bowed femora	+	NS	NS	NS	NS
Lobulated spleen	+	−	NS	NS	NS
Enlarged adrenal glands	+	−	NS	NS	NS
Hyperkalemic metabolic acidosis	NA	NA	NA	+	+
Increased serum creatine	NA	NA	NA	+	+

NS means not stated in clinical report, NA means not applicable, number of plus signs indicates the severity of the feature, and negative signs mean the feature is not present.

MATERIALS AND METHODS

Single Nucleotide Polymorphism (SNP) Array Analysis

Genomic DNA of both affected fetuses and their parents was genotyped with Affymetrix 250K arrays according to the manufacturer's protocols (Affymetrix, Santa Clara, CA). The 250K SNP genotypes were analyzed as described [de Leeuw et al., 2011].

TABLE II. Clinical Measurements

	Present family	
	II:1 (22 weeks)	**II:4 (16 weeks)**
Body parameters		
Body weight (g)	658 (461)	68.1 (108)
Crown-rump length (cm)	17.5 (19.3)	11 (12.4)
Crown-heel length (cm)	28 (28)	15 (17.5)
Head circumference (cm)	19.5 (19.4)	10.3 (12.4)
Organs (all in grams)		
Kidneys (left + right)	100 (4.6)	13.2 (0.9)
Lungs (left + right)	5.7 (13.1)	1.5 (3.9)
Liver	36.8 (25.5)	3.9 (5.9)
Heart	3.7 (3.1)	0.7 (0.8)
Adrenals	1.2 (1.9)	0.2 (0.6)

The normal weight or length at the indicated gestational week is given in parentheses.

Exome Sequencing

ES was performed essentially as described [Gilissen et al., 2010; Hoischen et al., 2010; Becker et al., 2011; Hoischen et al., 2011]. In brief, the exome enrichment was performed using a SureSelect v2 50Mb kit (Agilent, Santa Clara, CA), followed by sequencing on a SOLiD 5500xl System (Life Technologies, Foster City, CA). Read mapping and variant calling were performed using the LifeScope Software v2.1 (Life Technologies). Variant annotation was done using an in-house annotation pipeline. To prioritize variants in our sequencing data a quality filter was applied (>5 variant reads and >15% variant reads). Variants that were excluded were nongenic, intronic (except for canonical splice sites) or synonymous. Other variants that were excluded were present in dbSNPv130 or our in-house variants database that contains data from the 1000 Genomes Project as well as published variants and 133 in-house analyzed exomes. Candidate variants were validated by Sanger sequencing and segregation analysis.

Ethics approval was provided by the ethics review board of Arnhem-Nijmegen.

Histology

Renal and liver specimens from individual II:1 were stained with hematoxylin and eosin (H&E) in a semi-automatic manner using a Tissue-Tek Prisma from Sakura (Sakura Finetek, Torrance, CA). A renal specimen from individual II:1 was stained with periodic acid-Schiff (PAS) using the Special Stains Module from Roche (Roche Diagnostics International Ltd, Rotkreuz, Switzerland).

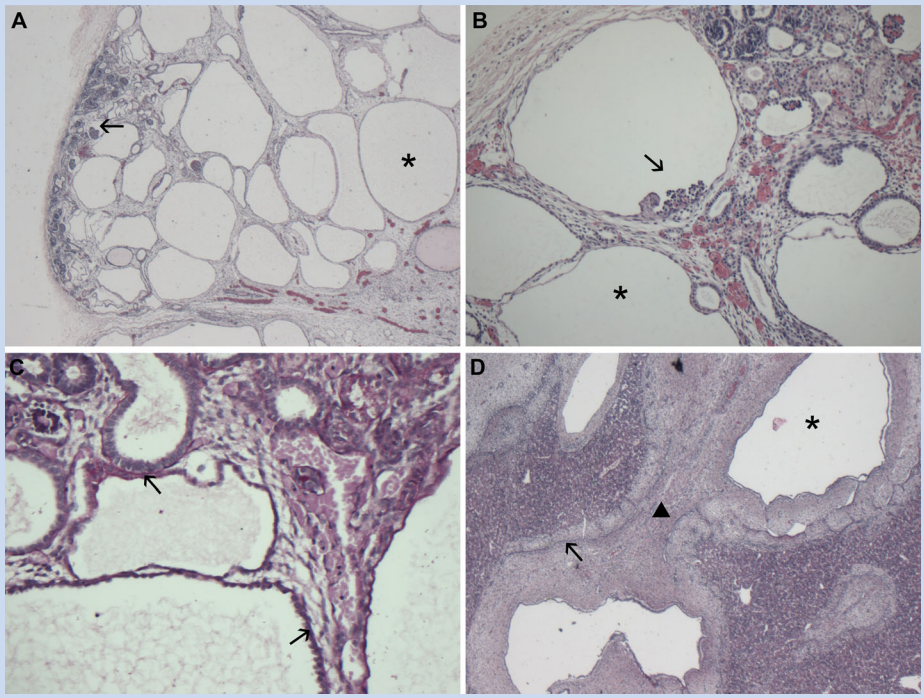

FIG. 2. Histological features of individual II:1. A, B: Renal cortex with cystic ductal structures indicated by the asterisk and dilated glomerular cysts indicated by the arrow (A, B: Hematoxylin and Eosin (H&E) staining; (A) 25× magnification; (B) 100× magnification). C: Periodic acid Schiff staining of the renal cortex showing the absence of significant tubular basement membrane thickening, indicated by the arrows (100× magnification). D: Liver section showing fibrosis indicated by the arrowhead, ductal plate malformation indicated by the arrow, and dilated cystic bile structures indicated by the asterisk (H&E staining; 50× magnification).

Immunocytochemistry

Fibroblasts from individual II:1 and control individuals were cultured on glass slides under standard cell culture conditions in Dulbecco's modified Eagle's medium (DMEM) with 20% fetal calf serum (FCS). Cilia formation was stimulated using serum-starved medium (DMEM with 0.2% FCS) for 48 hr prior to staining. Cells were then fixated in 2% paraformaldehyde in phosphate buffered saline (PBS) and permeabilized with 1% Trition-X-100 in PBS. Subsequently, the cells were blocked with freshly made 2% bovine serum albumin in PBS, followed by a 1-hr incubation with the primary antibody at room temperature. Cells were washed with PBS before incubation with the secondary antibody at room temperature for 45 min. The following primary antibodies were used: anti-inversin (rabbit polyclonal directed against amino acids 1–100; Protein tech, 1:100), anti-RPGRIP1L (guinea pig polyclonal; SN040, 1:500 [Arts et al., 2007]), and anti-acetylated α-tubulin (mouse monoclonal, Life Technologies, 1:1000). Secondary antibodies (all from Life Technologies) that were used: anti-guinea pig IgG Alexa Fluor 405 (1:300), anti-rabbit IgG Alexa Fluor 488 (1:300), and anti-mouse IgG Alexa Fluor 568 (1:300). Glass slides containing stained cells were embedded in Vectashield (Vector Laboratories, Burlingame, CA) on a microscopic glass slide. Microscopic analysis was performed on a Axio Imager ZI fluorescence microscope (Zeiss, Sliedrecht, The Netherlands) with an ApoTome slider. Images were processed using AxioVision (Zeiss) and Photoshop CS4 (Adobe Systems, San Jose, CA) software.

Reverse Transcriptase PCR and Quantitative PCR

cDNA was synthesized from fibroblast RNA using the iScript cDNA synthesis kit (Bio-Rad Laboratories, Hercules, CA) according to manufacturer's instructions. Reverse transcriptase PCR was conducted using primers for inversin cDNA spanning exons 11–13. PCR fragments were sequenced by Sanger sequencing. Quantitative PCR (qPCR) was conducted to quantitatively compare inversin mRNA expression in individual II:1 versus control individuals. qPCR analysis was performed on a 7900 Fast Real-Time PCR System (Applied Biosystems, Foster City, CA) with GoTaq PCR Master Mix (Promega, Madison, WI) according to the manufacturer's instructions. Primers were developed using the Primer 3 program (freely available online) and validated as described [de Brouwer et al., 2006]. *GUSB* was used as reference gene. qPCR quantifications were performed as described [Coene et al., 2011].

RESULTS

Homozygosity Mapping

Genome-wide homozygosity mapping using Affymetrix 250K arrays was conducted for individual II:1. Homozygosity analysis was performed as described by de Leeuw et al. [2011] using the loss of heterozygosity (LOH) algorithm at a threshold of 15.

Only a single homozygous region of 2.36 Mb was detected. This regions contained 16 annotated RefSeq genes with dbSNP rs16918660 (HG19 chr9:102,353,541) and rs10123826 (HG19 chr9:104,709,913) as bordering SNPs (see Supplemental Table SI for the genes in this region). The most likely candidate in this region was the *INVS* gene, which is associated with cystic kidney disease. To date, the other 15 genes have not been reported to be associated with a renal disorder.

Exome Sequencing

We applied ES to individual II:1 and targeted ~20,000 genes [Gilissen et al., 2010; Hoischen et al., 2010; Becker et al., 2011; Hoischen et al., 2011]. In total, 161,679,674 reads were obtained and 113,300,711 of them could be mapped to the human genome (HG19). In total, 41,811 variants were called in genes. Subsequently, these data were filtered for an autosomal recessive disease model, which yielded three homozygous variants and 11 compound heterozygous variants (see Supplemental Table SII for the variants). The variants were validated by Sanger sequencing and were checked for segregation of a recessive disease. All compound heterozygous variants were excluded as pathogenic because the unaffected mother I:2 carried the same combination of variants. Two of the variants that were initially marked as homozygous by ES were actually found by Sanger sequencing to be heterozygous in individual II:1. The last remaining homozygous variant, however, was confirmed. This indeed concerned the strong candidate gene *INVS* from our homozygosity mapping study (Fig. 3A), in which a previously unreported homozygous nonsense mutation in *INVS* was found at position c.1726C>T of NM_014425 (p.Arg576* of NP_055240). This mutation predicts the truncation of the IQ1 domain of the protein (Fig. 3D). However, nonsense-mediated decay is another potential consequence of this type of mutation. Inversin contains 16 ankyrin repeats, two IQ domains (IQ1 and IQ2, respectively), transcriptional regulator ICP4, a bipartite nuclear localization sequence, two D-box motifs, and a ninein homologous region. All homozygous nonsense mutations described in the literature thus far are located after the IQ1 domain (Fig. 3D).

RT-PCR and qPCR

We generated cDNA of invidual II:1 by reverse transcription PCR (RT-PCR) and Sanger sequencing showed the nonsense mutation c.1726C>T to be present in the RNA of individual II:1 (Fig. 3A). Quantitative PCR (qPCR) analysis showed a reduced level of *INVS* in fibroblasts of individual II:1 compared to two healthy control individuals (Fig. 3C).

Evaluation of the Ciliary Defect by Immunocytochemistry

In order to identify a potential ciliary defect in individual II:1, we evaluated cilia length, morphology, and localization of inversin by immunofluorescent staining of cilia in skin fibroblasts from the fetus, and from healthy control individuals. We were not able to detect a statistically significant difference in length nor morphology of the cilia in cells from individual II:1 compared to two control individuals (data not shown); however, the inversin localization appeared to be dramatically altered in cilia of individual II:1. In control fibroblasts, inversin localized to the ciliary axoneme in more than 50% of the cells, and in 25% of the cells we also detected inversin at the basal body. For individual II:1 inversin localized to the basal body in 30% of the cells, but inversin was completely absent from the ciliary axoneme (Fig. 3B).

DISCUSSION

NPHP is an autosomal recessive cystic kidney disease that is the most frequent monogenic cause of ESRD in children [Hildebrandt and Otto, 2005]. Two genes associated with infantile NPHP are *NPHP3* and *INVS* [Otto et al., 2003; Tory et al., 2009]. We found that mutations in the latter gene, *INVS*, caused the severe prenatal phenotype in the present family. This mutation was found through ES. The ES data were filtered for an autosomal recessive disease model and the candidate genes were, subsequently, checked for segregation within the family. The homozygous nonsense mutation in *INVS* at position c.1726C>T of NM_014425 was the only candidate left after segregation analysis within the family.

The phenotype of these fetuses is much more severe than in previously published reports of infantile NPHP and, because of the poor prognosis, led to termination of the pregnancies. Detailed phenotypic analysis showed a combination of grossly enlarged cystic kidneys, congenital liver fibrosis, and hypoplasia of the lungs associated with oligohydramnios. This is rarely seen in infantile NPHP, although Haider et al. [1998] previously described a large consanguineous family with NPHP including one individual who died shortly after birth due to respiratory failure. The causative mutation in this family was a homozygous nonsense mutation found in *INVS* at position c.2719C>T (found by Otto et al. [2003]), and the pregnancy of this individual was also complicated by oligohydramnios. A more detailed phenotypic characterization was, however, not included. Our combined data suggest that the co-occurrence of cystic kidneys and oligohydramnios is not compatible with life. The suspected skeletal abnormalities, these being shortening and mild bowing of the femora, have not been described in infantile NPHP before, but are a prominent feature of ciliopathy syndromes. These syndromes include asphyxiating thoracic dystrophy (OMIM 208500), cranioectodermal dysplasia (OMIM 218330), and short-rib polydactyly (OMIM 263530), and are caused by mutations in ciliary genes, such as genes encoding intraflagellar transport particle subunits (involved in retrograde axonemal transport in the cilium) [Huber and Cormier-Daire, 2012]. To date, causative mutations for these syndromes have never been found in *INVS*.

From a molecular point of view, it is known that inversin is important in left-right asymmetry during early embryonic development [Otto et al., 2003]. Inversin acts as a molecular switch between the canonical and non-canonical Wnt signaling pathways by its interaction with disheveled. A loss of function or absence of inversin will cause renal cyst formation by disruption of the balance between these two signaling pathways. Although the C-terminus of the protein is known to interact with disheveled, the exact epitope remains to be identified [Simons et al., 2005]. The nonsense mutation in the family reported here is localized in the IQ1 domain

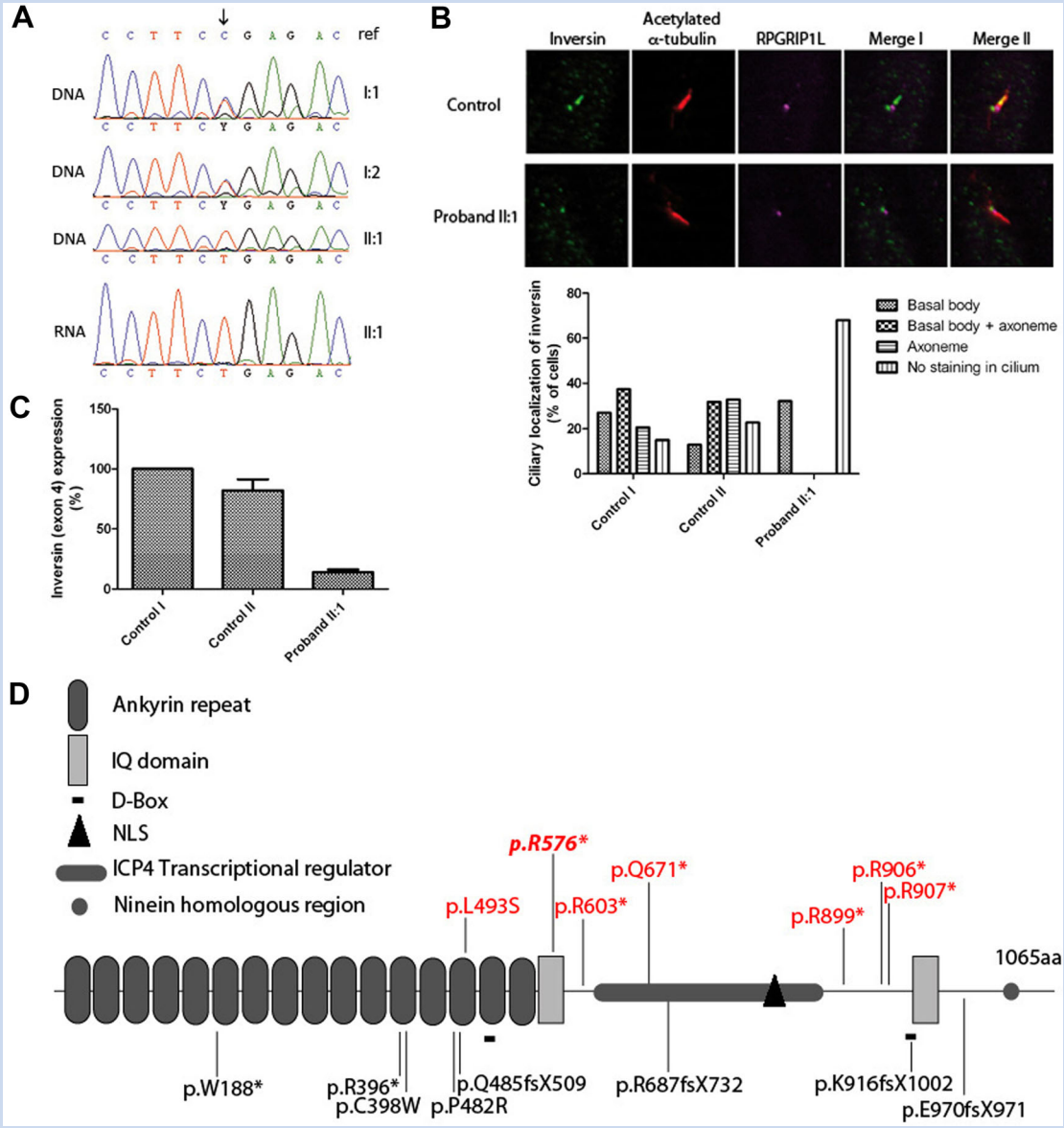

FIG. 3. Confirmation and evaluation of a novel nonsense mutation in *INVS*. A: Sequence of the homozygous nonsense mutation in *INVS* (NM_014425) at position c.1726C>T in fetus II:1, and the heterozygous state of the parents (I:1 and I:2), which fits the segregation of the disease. The bottom sequence shows the confirmation of the mutation in the RNA of fetus II:1. B: Immunofluorescent stainings of fibroblasts from a control individual and fetus II:1. Cilia were stained with a polyclonal antibody against inversin (shown in green), the ciliary axoneme is visualized by a monoclonal antibody against acetylated-α-tubulin (shown in red), and the ciliary transition zone is marked by a polyclonal antibody against RPGRIP1L (shown in purple). The fibroblasts of fetus II:1 show a mislocalization of inversin: in control fibroblasts, inversin is present in the previously described "inversin compartment" of the ciliary axoneme [Shiba et al., 2009] as well as at the basal body, whereas in the fibroblasts from the fetus, inversin can only be detected at the basal body. C: A reduction, but not absence, of inversin RNA in cDNA of fetus II:1 is detected by qPCR. D: A schematic representation of inversin (NP_055240) with its predicted motifs: 16 ankyrin repeats, two IQ domains, transcriptional regulator ICP4, a bipartite nuclear localization sequence, two D-box motifs, and one ninein homologous region [Lienkamp et al., 2012]. Mutations visualized in red were identified homozygously in patients, and mutations visualized in black were only found in a heterozygous state in combination with other heterozygous mutations [Otto et al., 2003; Tory et al., 2009; Chaki et al., 2011].

of inversin at position p.Arg576* (NP_055240). It is the most amino-terminal homozygous nonsense mutation in *INVS* reported in the literature for infantile NPHP. We show that although *INVS* RNA levels are significantly diminished in the patient-derived fibroblasts, likely due to nonsense-mediated decay, some mutated RNA remains present. Protein translated from this RNA is predicted to lack most of the protein including important motifs: IQ1 and IQ2, bipartite nuclear localization signals (NLS), destruction-

box (D-box) 2, and the ninein homologous region. Shiba et al. [2009] found that a 60 amino acid region at the C-terminus, including the ninein homologous region, is required for the localization of inversin to the ciliary axoneme. This finding supports our ciliary mislocalization results, that is, that mutant inversin solely localizes to the basal body and has lost its axonemal function. The exact roles of the other domains are still unknown, however, we do show that a truncation of the protein at the predicted IQ1 domain restricts the ciliary localization to the basal body.

In summary, we showed that the severe phenotypes of two fetuses with characteristics of infantile NPHP and Potter sequence were caused by a homozygous mutation in *INVS* at c.1726C>T of NM_014425 (p.Arg576*), which causes nonsense-mediated decay. Nonetheless, a small amount of mutant protein forms and mislocalizes to the basal body. The suspected skeletal abnormalities in the presented family may indicate that the phenotypic spectrum associated with *INVS* mutations is broader than presently thought, however, further investigation is required to gather complementary evidence to support this rationale.

ACKNOWLEDGMENTS

We thank members of the genomic disorders group Nijmegen for the technical support in performing the whole-exome sequencing. We thank C. Hall for useful discussions on the skeleton phenotype of individual II:1. This research was supported by grants from the Dutch Kidney Foundation (KJPB09.009 to H.H.A. and IP11.58 to H.H.A. and CP11.18 to N.V.A.M.K. and H.H.A.), the Netherlands Organization for Health Research and Development (ZonMW Veni-91612095 to A.H. and ZonMW Veni-91613008 to H.H.A.), and the Netherlands Organization for Scientific research (NWO Vidi-91786396 and Vici-016130664 to R.R.).

REFERENCES

Arts HH, Doherty D, van Beersum SE, Parisi MA, Letteboer SJ, Gorden NT, Peters TA, Marker T, Voesenek K, Kartono A, Ozyurek H, Farin FM, Kroes HY, Wolfrum U, Brunner HG, Cremers FP, Glass IA, Knoers NV, Roepman R. 2007. Mutations in the gene encoding the basal body protein RPGRIP1L, a nephrocystin-4 interactor, cause Joubert syndrome. Nat Genet 39:882–888.

Arts HH, Knoers NV. 2012. Current insights into renal ciliopathies: What can genetics teach us? Pediatr Nephrol 28:863–874.

Becker J, Semler O, Gilissen C, Li Y, Bolz HJ, Giunta C, Bergmann C, Rohrbach M, Koerber F, Zimmermann K, de Vries P, Wirth B, Schoenau E, Wollnik B, Veltman JA, Hoischen A, Netzer C. 2011. Exome sequencing identifies truncating mutations in human SERPINF1 in autosomal-recessive osteogenesis imperfecta. Am J Hum Genet 88:362–371.

Chaki M, Hoefele J, Allen SJ, Ramaswami G, Janssen S, Bergmann C, Heckenlively JR, Otto EA, Hildebrandt F. 2011. Genotype-phenotype correlation in 440 patients with NPHP-related ciliopathies. Kidney Int 80:1239–1245.

Coene KL, Mans DA, Boldt K, Gloeckner CJ, van Reeuwijk J, Bolat E, Roosing S, Letteboer SJ, Peters TA, Cremers FP, Ueffing M, Roepman R. 2011. The ciliopathy-associated protein homologs RPGRIP1 and RPGRIP1L are linked to cilium integrity through interaction with Nek4 serine/threonine kinase. Hum Mol Genet 20:3592–3605.

de Brouwer AP, van Bokhoven H, Kremer H. 2006. Comparison of 12 reference genes for normalization of gene expression levels in Epstein-Barr virus-transformed lymphoblastoid cell lines and fibroblasts. Mol Diagn Ther 10:197–204.

de Leeuw N, Hehir-Kwa JY, Simons A, Geurts van Kessel A, Smeets DF, Faas BH, Pfundt R. 2011. SNP array analysis in constitutional and cancer genome diagnostics—Copy number variants, genotyping and quality control. Cytogenet Genome Res 135:212–221.

Gagnadoux MF, Bacri JL, Broyer M, Habib R. 1989. Infantile chronic tubulo-interstitial nephritis with cortical microcysts: Variant of nephronophthisis or new disease entity? Pediatr Nephrol 3:50–55.

Gilissen C, Arts HH, Hoischen A, Spruijt L, Mans DA, Arts P, van Lier B, Steehouwer M, van Reeuwijk J, Kant SG, Roepman R, Knoers NV, Veltman JA, Brunner HG. 2010. Exome sequencing identifies WDR35 variants involved in Sensenbrenner syndrome. Am J Hum Genet 87:418–423.

Haider NB, Carmi R, Shalev H, Sheffield VC, Landau D. 1998. A Bedouin kindred with infantile nephronophthisis demonstrates linkage to chromosome 9 by homozygosity mapping. Am J Hum Genet 63:1404–1410.

Halbritter J, Porath JD, Diaz KA, Braun DA, Kohl S, Chaki M, Allen SJ, Soliman NA, Hildebrandt F, Otto EA, Group GPNS. 2013. Identification of 99 novel mutations in a worldwide cohort of 1,056 patients with a nephronophthisis-related ciliopathy. Hum Genet 132:865–884.

Hildebrandt F, Otto E. 2005. Cilia and centrosomes: A unifying pathogenic concept for cystic kidney disease? Nat Rev Genet 6:928–940.

Hoischen A, van Bon BW, Gilissen C, Arts P, van Lier B, Steehouwer M, de Vries P, de Reuver R, Wieskamp N, Mortier G, Devriendt K, Amorim MZ, Revencu N, Kidd A, Barbosa M, Turner A, Smith J, Oley C, Henderson A, Hayes IM, Thompson EM, Brunner HG, de Vries BB, Veltman JA. 2010. De novo mutations of SETBP1 cause Schinzel–Giedion syndrome. Nat Genet 42:483–485.

Hoischen A, van Bon BW, Rodriguez-Santiago B, Gilissen C, Vissers LE, de Vries P, Janssen I, van Lier B, Hastings R, Smithson SF, Newbury-Ecob R, Kjaergaard S, Goodship J, McGowan R, Bartholdi D, Rauch A, Peippo M, Cobben JM, Wieczorek D, Gillessen-Kaesbach G, Veltman JA, Brunner HG, de Vries BB. 2011. De novo nonsense mutations in ASXL1 cause Bohring–Opitz syndrome. Nat Genet 43:729–731.

Huber C, Cormier-Daire V. 2012. Ciliary disorder of the skeleton. Am J Med Genet C Semin Med Genet 160C:165–174.

Hurd TW, Hildebrandt F. 2011. Mechanisms of nephronophthisis and related ciliopathies. Nephron Exp Nephrol 118:e9–e14.

Lienkamp S, Ganner A, Walz G. 2012. Inversin, Wnt signaling and primary cilia. Differentiation 83:S49–S55.

Otto EA, Schermer B, Obara T, O'Toole JF, Hiller KS, Mueller AM, Ruf RG, Hoefele J, Beekmann F, Landau D, Foreman JW, Goodship JA, Strachan T, Kispert A, Wolf MT, Gagnadoux MF, Nivet H, Antignac C, Walz G, Drummond IA, Benzing T, Hildebrandt F. 2003. Mutations in INVS encoding inversin cause nephronophthisis type 2, linking renal cystic disease to the function of primary cilia and left-right axis determination. Nat Genet 34:413–420.

Saunier S, Salomon R, Antignac C. 2005. Nephronophthisis. Curr Opin Genet Dev 15:324–331.

Shiba D, Yamaoka Y, Hagiwara H, Takamatsu T, Hamada H, Yokoyama T. 2009. Localization of Inv in a distinctive intraciliary compartment requires the C-terminal ninein-homolog-containing region. J Cell Sci 122:44–54.

Simons M, Gloy J, Ganner A, Bullerkotte A, Bashkurov M, Kronig C, Schermer B, Benzing T, Cabello OA, Jenny A, Mlodzik M, Polok B,

Driever W, Obara T, Walz G. 2005. Inversin, the gene product mutated in nephronophthisis type II, functions as a molecular switch between Wnt signaling pathways. Nat Genet 37:537–543.

Thomas IT, Smith DW. 1974. Oligohydramnios, cause of the nonrenal features of Potter's syndrome, including pulmonary hypoplasia. J Pediatr 84:811–815.

Tory K, Rousset-Rouviere C, Gubler MC, Moriniere V, Pawtowski A, Becker C, Guyot C, Gie S, Frishberg Y, Nivet H, Deschenes G, Cochat P, Gagnadoux MF, Saunier S, Antignac C, Salomon R. 2009. Mutations of NPHP2 and NPHP3 in infantile nephronophthisis. Kidney Int 75:839–847.

SUPPORTING INFORMATION

Additional supporting information may be found in the online version of this article at the publisher's web-site.